INFLUENCE OF CARBON CONTENT ON WORKABILITY BEHAVIOUR IN THE FORMATION OF SINTERED PLAIN CARBON STEEL PREFORMS

[1]S. Narayan* [2]A. Rajeshkannan

*** Corresponding Author**

[1]Mr. SUMESH NARAYAN

Assistant Lecturer, Mechanical Engineering,
School of Engineering and Physics,
Faculty of Science, Technology & Environment,
The University of the South Pacific, Laucala Campus,
PO Box 1168, Suva, FIJI.
Off. No. +679 3232034,
Fax No. +679 3231538,
Email: narayan_su@usp.ac.fj

Co-Author

[2]Dr. ANANTHANARAYANAN RAJESH KANNAN

Lecturer, Mechanical Engineering,
School of Engineering and Physics,
Faculty of Science, Technology & Environment,
The University of the South Pacific, Laucala Campus,
PO Box 1168, Suva, FIJI.
Off. No. +679 3232695,
Fax No. +679 3231538,
Email: ananthanarayanan_r@usp.ac.fj

Abstract

Complete experimental investigation on the workability behaviour of sintered plain carbon steel cylindrical preforms with carbon contents of 0%, 0.35%, 0.75% and 1.1%, under cold upsetting, have been studied in order to understand the influence of carbon content on the workability process. The abovementioned powder metallurgy sintered preforms with constant initial theoretical density of 84% and aspect ratio of 0.4 were prepared using a suitable die–set assembly on a 1 MN capacity hydraulic press and sintered for 90 minutes at 1200 ^{o}C. Each sintered preform was cold upset under nil/no frictional constraint. Under triaxial stress state condition densification, axial stress, hoop stress, hydrostatic stress, effective stress and formability stress index against axial strain relationship was established and presented in this work. Further, attained density is considered to establish formability stress index and various stress ratio parameters behaviour.

Keywords*: Workability; Stress ratio parameter; Formability stress index.*

1. Introduction

Powder metallurgy (P/M) process is a near-net or net-shape production technology and is attractive as it blends cost and material saving advantage compared to other conventional manufacturing processes. The distinctive features obtained by P/M processes are cost reduction, improvement in performance, tailor made design, greater accuracy, high precision, better surface finish, and homogeneity of structure and the production of unique materials [1, 2]. Some typical applications of P/M parts are parts with porosity such as filters, permanently lubricating bearings, in which air pores in P/M part are filled with oil via secondary process of impregnation, parts of certain metals or metal alloys that are difficult to fabricate by other methods and parts of materials with special and unique properties. Preforms are prepared in various steps that involve powder mixing, compacting and sintering known as primary deformation processes. A known limitation of this route is the residual porosity left in preforms after the sintering process. A secondary deformation process is used in order to enhance the properties of sintered powder materials. Secondary processes such as pressing or repressing, powder extrusion, powder rolling, and infiltration can be used to improve the mechanical properties of parts produced through conventional powder metallurgy route [3-5]. The workability or formability of the P/M material plays a major role in determining if the P/M material will be formed successfully or fracture initiates in the forming process. Workability is a measure of the extent of deformation that a material can withstand due to the induced internal stresses of forming prior to fracture and is not only dependent on the material but also on several forming parameters such as stress and strain rate, friction, temperature, etc [6-8].

Several constitutive equations have been proposed and studied to understand the constitutive behaviour of materials during forming operations [9-12]. Later Abdel-Rahman and El-Sheikh [7], investigating the effect of relative density on the forming limit of P/M materials also proposed the stress formability criteria (β) for describing the effect of mean stress and the effective stress by employing theories proposed by Kuhn-Downey [13] and Whang-Kobayashi [4]. It has been reported [14, 15] that different fracture mechanisms are present depending on the amount of triaxiality and the equivalent strain and stress triaxiality were important parameters that govern the crack formation. Deformation control to avoid fracture can be established by careful selection of process parameters, the factors being die shaping, lubrication, preform shape, preform dimensions and density. Geometrical design of the preform in metal forging of complex parts has great effects on the forging load and plays a key role in improving product quality such as ensuring defect-free product and proper metal flow. The formability limit of powder metallurgy material is usually determined by visible crack initiation on the free surface. By careful selection of process parameter and deformation process, densification can be enhanced and crack appearance on the deforming preforms can be avoided by increasing the compressive level of stresses on the material [16-18]. Lubrication also plays an important role in metal flow particularly in cold upsetting as it affects the densification and forming limit mechanisms. A good lubrication improves the quality of products through the reduction of defects and improvement in the dimensional accuracy and surface finish [19-21]. Narayanasamy et al. [22] had presented the microstructure of pure iron, Fe-0.4%C and Fe-0.8%C and showed that as the smaller carbon particle size increases in the preform the pore size reduces. Further, they reported better densification for carbon steels compared to pure iron. Thus, the present investigation is aimed to

establish the workability behaviour under triaxial stress state condition of powder metallurgy preforms of pure iron, Fe-0.35%C, Fe-0.75%C and Fe-1.1%C experimentally under nil/no lubricant condition and constant aspect ratio of 0.4. It was also desired to establish the technical relationship that exists between the characteristics of axial stress, hoop stress, hydrostatic stress, effective stress and formability stress index with respect to true height strain and densification. Further, the technical relationship was established which exists between stress ratio parameters namely ($\sigma_\theta / \sigma_{eff}$), ($\sigma_m / \sigma_{eff}$) and ($\sigma_z / \sigma_{eff}$) with respect to percent fractional theoretical density and axial strain.

2. Experimental details

2.1 Materials and characterization

Atomized iron powder of less than or equal to 150 µm size and graphite powder of 2-3 µm size were used in the present investigation. Analysis indicated that the purity of iron was 99.7 percent and the rest were insoluble impurities. The characteristic (apparent density, flow rate and particle size distribution) of iron powder, Fe-0.35%C, Fe-0.75%C and Fe-1.1%C blends are shown in Tables 1 and 2.

Table 1: Characterization of iron powder

Si. No.	Property	Iron	Fe-0.35%C Blend	Fe-0.75%C Blend	Fe-1.1%C Blend
1.	Apparent Density (g/cc)	3.38	3.37	3.29	3.21
2.	Flow rate, (s/50g) by Hall Flow Meter	26.3	28.1	25.3	24.8
3.	Compressibility (g/cc) at pressure of 430±10MPa	6.46	6.26	6.41	6.35

Table 2: Sieve size analysis of iron powder.

Sieve size (µm)	150	+125	+100	+75	+63	+45	-45
Wt % Ret.	10.60	24.54	15.46	19.90	11.10	8.40	10.00

2.2 Blending, compaction and sintering

A powder mix corresponding to Fe-0%C, Fe-0.35%C, Fe-0.75%C and Fe-1.1%C was taken in a stainless steel pot with the powder mixed to porcelain balls (10 mm – 15 mm diameter) with a ratio of 1:1 by weight. The pot containing the blended powder was subjected to the blending operation by securely tightening and then fixing it to the pot mill. The mill was operated for 20 hours to obtain a homogenous mix. Green compacts of 28 mm diameter with 12 mm of length were prepared. The powder blend was compacted on a 1.0 MN hydraulic press using a suitable die, a punch and a bottom insert in the pressure range of 430 ± 10 MPa to obtain an initial theoretical density of 0.84 ± 0.01. In order to avoid oxidation during sintering and cooling, the entire surface of the compacts were indigenously formed ceramic coated. These ceramic coated compacts were heated in the

electric muffle furnace with temperature of 1200 ^{0}C ± 10 ^{0}C. At this temperature the compacts were sintered for 90 minutes followed by furnace cooling.

2.3 Cold deformation

Sintered and furnace cooled preforms were machined to such a dimension so as to provide height–to–diameter ratio of 0.40. The initial dimensions of the cylindrical preforms were measured, recorded, and used to calculate the initial density. Each specimen was compressively deformed between a flat die-set in the incremental loading step of 0.05 MN using 1 MN capacity hydraulic press under friction condition, which included dry, unlubricated dies called nil/no lubricant condition. The deformation process was stopped once a visible crack appeared at the free surface. Dimensional measurements such as deformed height, deformed diameters (including bulged and contact) were carried out after every step of deformation using digital vernier caliper and the density measurements being carried out using Archimedes principle. Experimental results were used to calculate the axial stress, hoop stress, hydrostatic stress, effective stress, various stress ratio parameters namely $(\sigma_\theta / \sigma_{eff})$, $(\sigma_m / \sigma_{eff})$ and $(\sigma_z / \sigma_{eff})$, true height strain, percentage theoretical density and formability stress index.

3. Theoretical analysis

The plastic deformation behaviour of porous metals is influenced by the internal pores and the analysis of porous metals requires an appropriate yield criterion which should take the pore effect into account. Many researchers over the years have analyzed several different yield criteria for sintered powder materials which are based on experimental and theoretical analysis [9, 23-24]. A typical theorem is

that the plastic deformation occurs when the elasticity strain energy reaches a critical value. The formulation can be written as

$$AJ_2^{/} + BJ_1^2 = Y^2 = \delta Y_0^2 \tag{1}$$

where *A, B,* δ are yield criterion parameters and are functions of relative density, J_1 is the first invariant of the stress tensor, $J_2^{/}$ is the second invariant of the stress deviator and Y_0 and Y are yield strength of a solid and partially dense material having relative density *R*, respectively [24]. The parameters J_1 and $J_2^{/}$ in the cylindrical coordinate system where the axis represents radial, circular and axial direction can be expressed as follows

$$J_2^{/} = \frac{1}{6}\left[(\sigma_r - \sigma_\theta)^2 + (\sigma_\theta - \sigma_z)^2 + (\sigma_z - \sigma_r)^2\right] \tag{2}$$

$$J_1 = \sigma_r + \sigma_\theta + \sigma_z \tag{3}$$

Here for axisymmetric forging, $\sigma_r = \sigma_\theta$, $J_2^{/}$ and J_1^2 can be written as

$$J_2^{/} = \frac{1}{6}\left(2\sigma_\theta^2 + 2\sigma_z^2 - 4\sigma_\theta\sigma_z\right) \tag{4}$$

$$J_1^2 = 4\sigma_\theta^2 + \sigma_z^2 + 4\sigma_\theta\sigma_z \tag{5}$$

Substituting Eq. (4) and Eq. (5) into Eq. (1) gives

$$\frac{A}{6}\left(2\sigma_\theta^2 + 2\sigma_z^2 - 4\sigma_\theta\sigma_z\right) + B\left(4\sigma_\theta^2 + \sigma_z^2 + 4\sigma_\theta\sigma_z\right) = \delta Y_0^2 \tag{6}$$

Qin and Hua [9] have investigated and presented the values for yield criterion parameters based on plastic Poisson's ratio, relative density and flow stress of the matrix material and several yield criterions for sintered powder material were also compared with each other. The following yield criteria parameters are chosen in this research as $A = 2 + R^2$, $B = (1 - R^2)/3$, $\delta = [(R - R_0)/(1 - R_0)]^2$. Eq. (6) can now be written as

$$Y_0 = \sigma_{eff} = \left[\frac{(1-R_0)^2(\sigma_z^2 + 2\sigma_\theta^2 - R^2(\sigma_\theta^2 + 2\sigma_\theta\sigma_z))}{(R-R_0)^2} \right]^{0.5} \quad (7)$$

Eq. (7) gives the expression for effective stress in terms of cylindrical coordinates. According to Narayansamy et al. [6], the state of stress in a triaxial stress condition is given by

$$\alpha = \frac{(2+R^2)\sigma_\theta - R^2(\sigma_z + 2\sigma_\theta)}{(2+R^2)\sigma_z - R^2(\sigma_z + 2\sigma_\theta)} \quad (8)$$

Using Eq. (8) for the values of Poisson's ratio (α), relative density (R) and axial stress (σ_z) the hoop stress (σ_θ) under triaxial stress state condition can be determined as given below:

$$\sigma_\theta = \left[\frac{2\alpha + R^2}{2 - R^2 + 2R^2\alpha} \right] \sigma_z \quad (9)$$

where, $\alpha = \frac{d\varepsilon_\theta}{d\varepsilon_z}$

The stress formability factor [7] is given as

$$\beta = \frac{J_1}{(3J_2^{/})^{0.5}} = \frac{3\sigma_m}{\sigma_{eff}}, \quad (10)$$

where, $\sigma_m = \frac{\sigma_r + \sigma_\theta + \sigma_z}{3} = \frac{2\sigma_\theta + \sigma_z}{3}$, is the hydrostatic stress.

The stress formability factor as expressed in Eq. (10) is used to describe the effect of mean stress and the effective stress on the forming limit of P/M compacts in upsetting.

4. Results and discussion

Figures 1 and 2 show the variation of formability stress index against true height strain and relative density, respectively. The initial theoretical density, aspect ratio

and frictional constraints are kept constant at 84 percent, 0.4 and nil/no lubricant respectively. Consequently, the effect of carbon content on the formability of selected plain carbon steel is investigated here. It is seen for all preforms that axial strain and percent theoretical density increases with increasing value of formability stress index, however, the formability stress index decreases with decreasing carbon content in the preform for a given true height strain (Fig. 1). The formability stress index value for Fe-1.1%C takes a significantly high value in comparison to other preforms where the final formability stress index achieved are almost same, however, this occurred at different fracture strain values. From Fig. 2 it is evident that the effect of carbon content on formability stress index is literally nil, however, an enhanced formability stress index value is obtained for Fe-1.1%C deformed under nil/no lubricant condition.

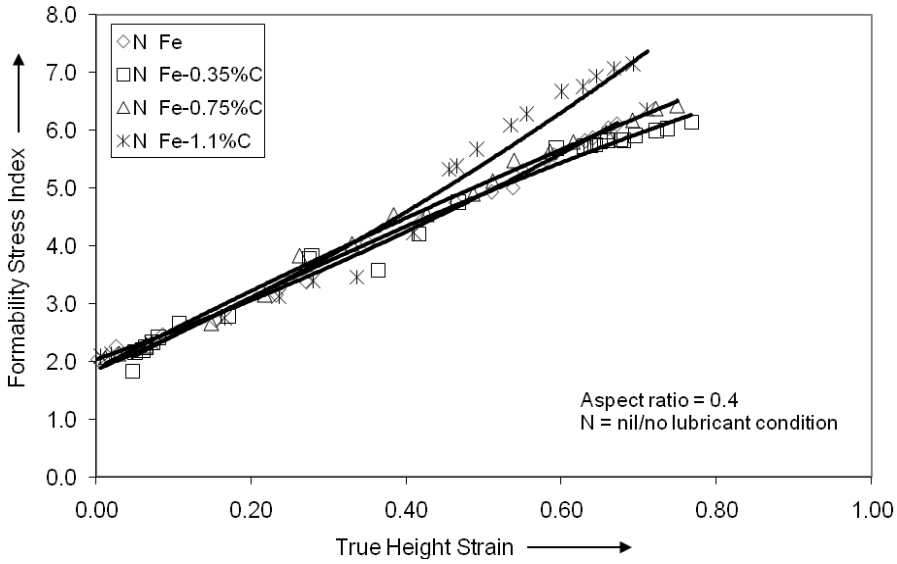

Fig. 1: Relationship between formability stress index and true height strain.

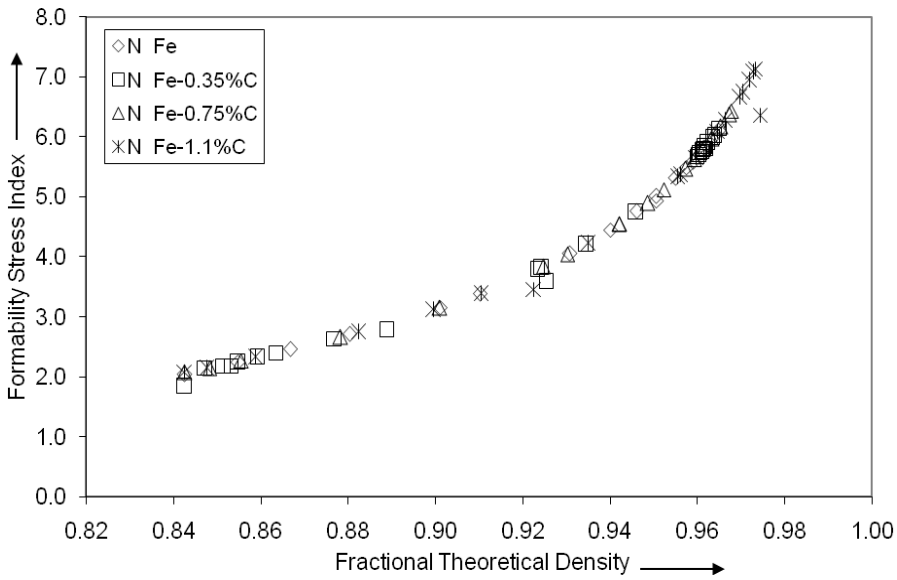

Fig. 2: Relationship between formability stress index and fractional theoretical density.

Fig. 3 is plotted to show the relationship between fractional theoretical density and true height strain for plain carbon steel preforms cold deformed with 0.4 aspect ratio. The percentage of carbon content in the preform varied from 0 to 1.1 percent. Further, the effect of carbon content on the densification behaviour is discussed here. Up to 0.4 true height strain the densification rate is highest in pure iron preform and the densification rate decreases with increasing carbon content in the preform. Further, after 0.4 true height strain the densification rate in Fe-1.1%C preform is found to be the highest, however, the densification rate reduces with reducing carbon content in the preform. Apart from iron-to-iron bonding the carbon particles diffuse into the ferrous matrix during the sintering process. Further, another important factor affecting the properties of the sintered steel preform is the combination of carbon with iron particles. The above phenomenon together with shrinkage during sintering process affects the pore size in the plain carbon steel preforms studied during this research and as the carbon content increases the pore size in the preforms reduces which are difficult to deform than larger size pores, hence, the densification rate is enhanced for pure iron during

initial stages of deformation as larger pores are more easily collapsed and closed. Further, as the lateral deformation is more pronounced the larger pores present in pure iron are more elongated in the direction of metal flow than the smaller pores present in the iron carbon alloy preforms. Hence, the pores present in iron carbon alloy are more effectively closed and maybe the reason for higher densification rate for 1.1 percent carbon preform after 0.4 true height strain.

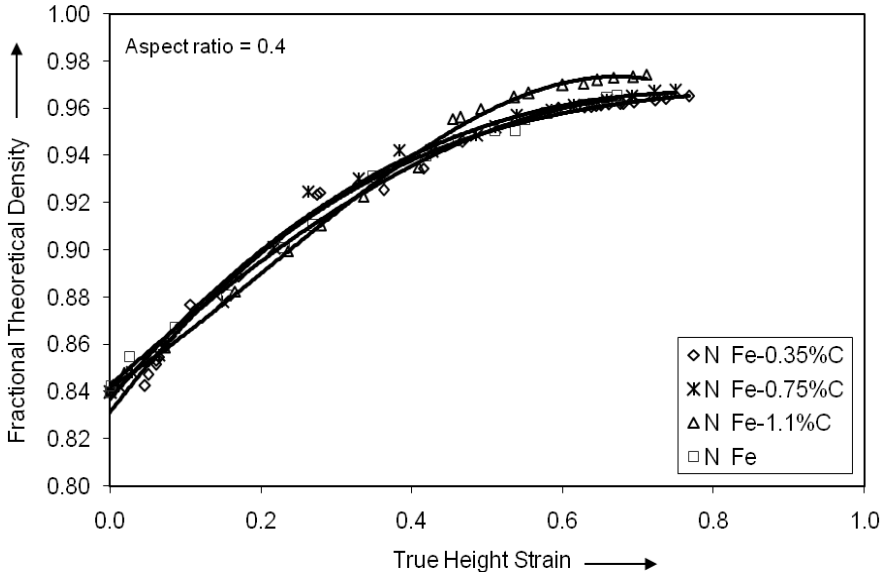

Fig. 3: Relationship between fractional theoretical density and true height strain.

Fig. 4 is plotted to show the relationship between axial stress and true height strain for plain carbon steel preforms cold deformed with 0.4 aspect ratio. The percentage of carbon content in the preform varied from 0 to 1.1 percent. For any given true height strain the flow stress increases with the increasing percentage of carbon content in the preform. It is clearly evident that the stress values after 0.2 true height strain are higher for Fe-1.1%C in comparison to other preforms, hence, it can be said that increasing the carbon content in the preform has enhanced the stress values for further deformation. Also, the lateral deformation is found to be lower for high carbon content preform which may be one of the reasons for higher

stress value for 1.1 percent carbon preform. Further, a steep rise in the stress values for pure iron is observed during the final stages of deformation indicating that strain hardening is faster and higher in pure iron preform. Fig. 5 is plotted to show the relationship between hydrostatic, axial and hoop stresses against true height strain for pure iron preform. The difference between hydrostatic stress, hoop stress and axial stress is literally nil against true height strain, and hence, the behaviour is similar to that discussed earlier between axial stress and true height strain.

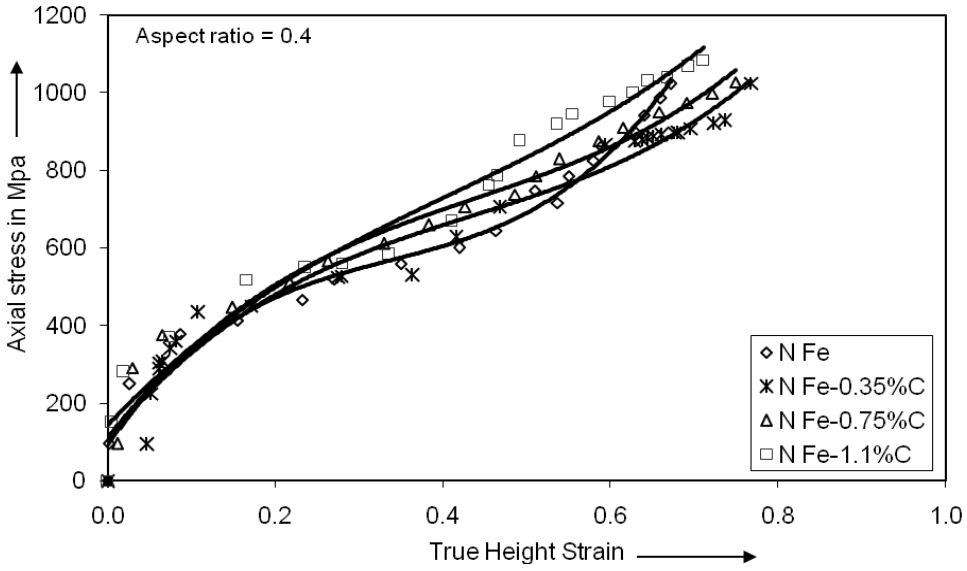

Fig. 4: Variation of axial stress against true height strain.

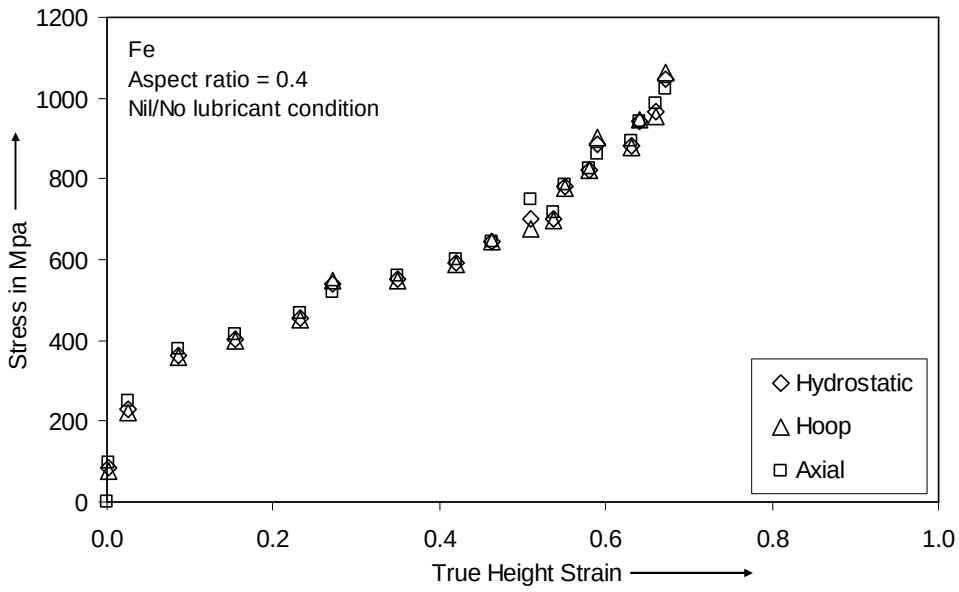

Fig. 5: Variation of hydrostatic, hoop and axial stresses against true height strain.

Fig. 6 is plotted to show the relationship between effective stress and true height strain for plain carbon steel preforms cold deformed with 0.4 aspect ratio. The percentage of carbon content in the preform varied from 0 to 1.1 percent. It can be seen that the effective stress increases rapidly for low true height strain values followed by gradual decrease upto a height strain of approximately 0.5 and thereafter remains almost constant until fracture. For any given true height strain the effective stress is found to be the highest in 1.1 percent carbon preform, however, after 0.5 true height strain the difference in the effective stress values are literally nil.

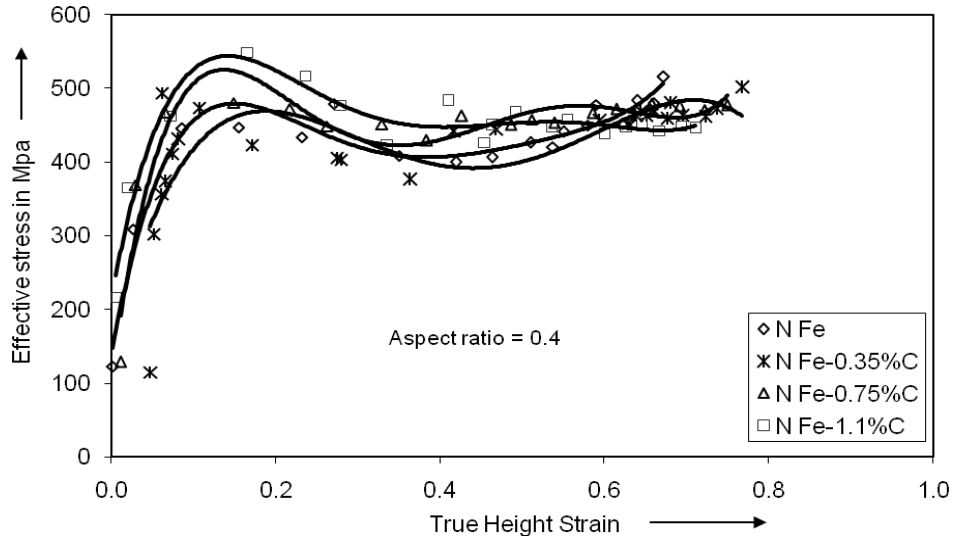

Fig. 6: Variation of effective stress against true height strain

Fig. 7 shows the relationship of stress ratio parameter, σ_z / σ_{eff} against relative density under the influence of carbon content in the preforms. The aspect ratio is kept constant at 0.4. The characteristics nature of the curves plotted are similar and as the densification increases the stress ratio parameter, σ_z / σ_{eff}, also increases. As seen from Fig. 7 the effect of carbon content on the stress ratio parameter, σ_z / σ_{eff}, is literally nil, however, an improved final value of σ_z / σ_{eff} is observed for Fe-1.1%C preform under nil/no lubricant condition. Fig. 8 is plotted to show the relationship between several stress ratio parameters namely, $\sigma_\theta / \sigma_{eff}$, σ_m / σ_{eff} and σ_z / σ_{eff} against relative density. It is seen that the difference between the above mentioned stress ratio parameters plotted against relative density is literally nil, and hence, the behaviour is similar to that discussed earlier between σ_z / σ_{eff} and relative density.

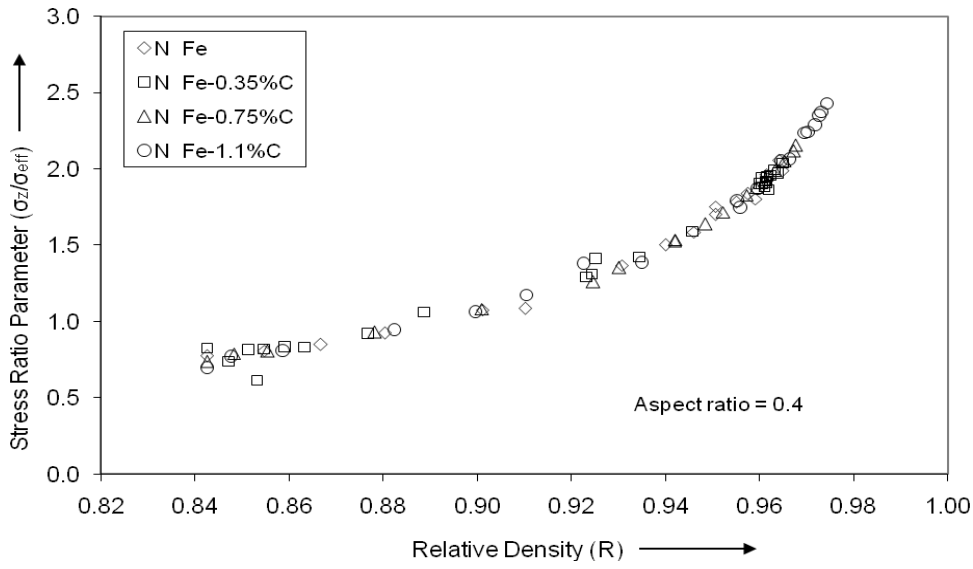

Fig. 7: Variation of stress ratio parameter, σ_z / σ_{eff} against relative density.

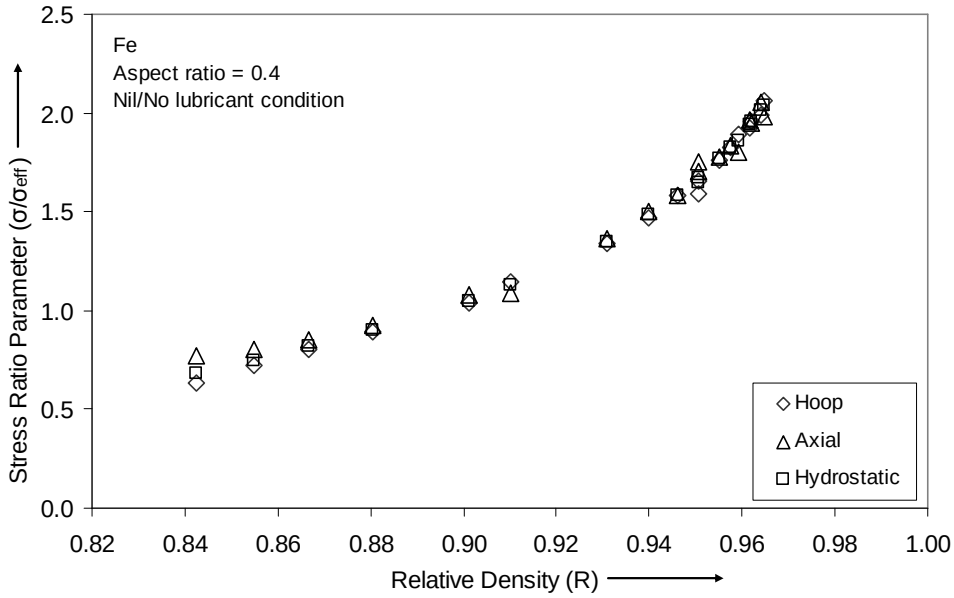

Fig. 8: Variation of stress ratio parameter ($\sigma_\theta / \sigma_{eff}$), (σ_m / σ_{eff}) and (σ_z / σ_{eff}) against relative density.

Fig. 9 shows the relationship of stress ratio parameter, σ_z / σ_{eff} against true height strain under the influence of carbon content. The aspect ratio is kept constant at 0.4 and the preforms are cold upset forged under nil/no lubricant condition. For all preforms with different carbon content, the axial strain increases as increasing value of stress ratio parameter, σ_z / σ_{eff}. It is seen that the stress ratio

parameter, σ_z / σ_{eff} values decrease with decreasing carbon content in the preform for a given true height strain value. For Fe-1.1%C, the stress ratio parameter, σ_z / σ_{eff} takes a very high value at the fracture strain. The above findings of higher stress ratio parameter, σ_z / σ_{eff} value for Fe-1.1%C preform is due to the closure of very fine pores. Further, for pure iron, Fe-0.35%C and Fe-0.75%C the final stress ratio parameter, σ_z / σ_{eff} achieved is almost the same, however at different strain values. Fig. 10 is plotted to show the relationship between several stress ratio parameters namely, $\sigma_\theta / \sigma_{eff}$, σ_m / σ_{eff} and σ_z / σ_{eff} against axial strain. It is seen that the difference between the above mentioned stress ratio parameters plotted against axial strain is literally nil, and hence, the behaviour is similar to that of discussed earlier between σ_z / σ_{eff} and axial strain.

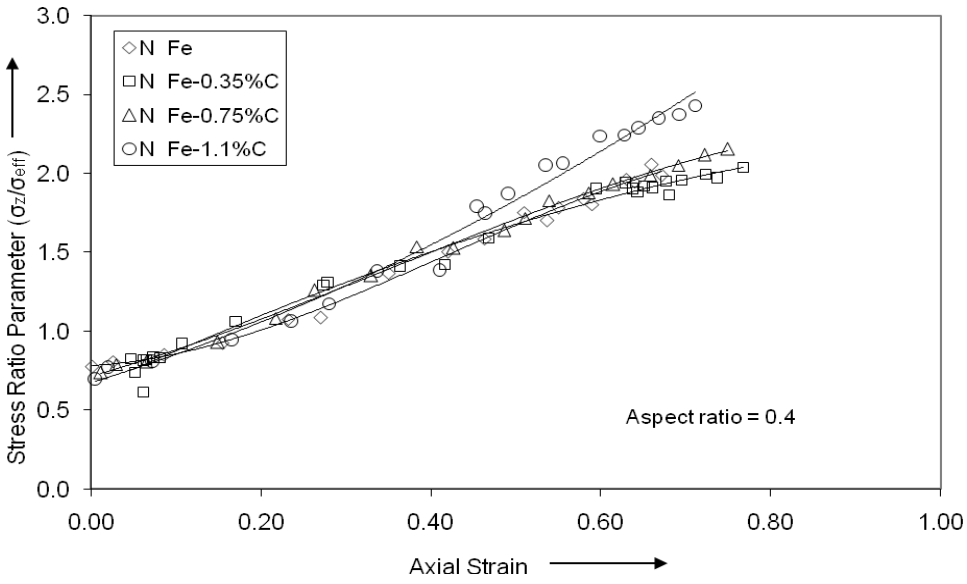

Fig. 9: Variation of stress ratio parameter, σ_z / σ_{eff} against axial strain.

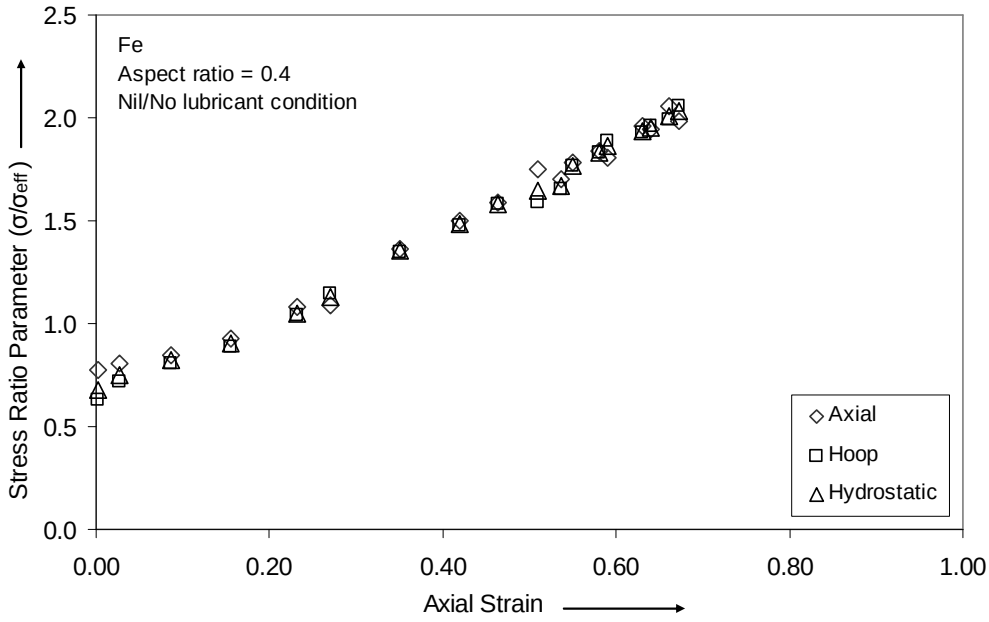

Fig. 10: Variation of stress ratio parameter ($\sigma_\theta / \sigma_{eff}$), (σ_m / σ_{eff}) and (σ_z / σ_{eff}) against axial strain.

5. Conclusions

From the present investigation it is seen that different percentages of carbon content in the powder metallurgy preforms have significant implications on the workability behaviour and the major conclusions have been drawn that are as follows:

- Increasing the carbon content in iron increases the overall densification and the amount of densification at any given axial strain, further it is evident that other workability parameters like formability stress index, axial, hoop, hydrostatic and effective stresses are enhanced with the enhancing level of carbon content.
- The difference observed between axial stress, hydrostatic stress and hoop stress against axial strain is literally nil irrespective of the compositions. Also the effect of stress ratio parameters ($\sigma_\theta / \sigma_{eff}$, σ_m / σ_{eff} and σ_z / σ_{eff})

against induced strain and promoted densification is practically negligible for all the concerned preforms.

References

1. Huang CC, Cheng JH (2004) An investigation into the forming limits of sintered porous materials under different operational conditions. J Mater Process Technol 148:382-393.
2. Chandramouli R, Pandey KS, Kandavel TK, Ashokkumar T, Shanmugasundaram D (2007) Influence of material flow constraints during cold forming on the deformation and densification behaviour of hypoeutectoid P/M steel ring preforms. Int J Adv Mfg Technol 31:926-932.
3. Zhang XQ, Peng YH, Li MQ, Wu SC, Ruan XY (2000) Study of workability limits of porous materials under different upsetting conditions by compressible rigid plastic finite element method. J Mater Engng Perform 9:164-169.
4. Whang BB, Kobayashi S (1990) Deformation characterization of powdered compacts in compaction. Int J Mach Tools Mfg 30:309-323.
5. Kandavel TK, Chandramouli R, Ravichandran M (2010) Experimental study on the plastic deformation and densification characteristics of some sintered and heat treated low alloy powder metallurgy steels. Mater Des 31:485-492.
6. Narayanasamy R, Ramesh T, Pandey KS (2005) Some aspects on workability of aluminium-iron powder metallurgy composite during cold upsetting. Mater Sci Eng A 391:418-426.
7. Rahman MA, El-Sheikh MN (1995) Workability in forging of powder metallurgy compacts. J Mater Process Technol 54:97-102
8. El-Domiatry A, Shaker M (1991) A note on the workability of porous-steel preforms. J Mater Process Technol 25:229-233.
9. Qin XP, Hua L (2007) Deformation and strengthening of sintered ferrous material. J Mater Process Technol 188:694-697.
10. Kuhn HA (1978) Powder Metallurgy Processing. Academic press, New York.
11. Taha MA, El-Mahallawy NA, El-Sabbagh AM (2008) Some experimental data on workability of aluminium-particulate-reinforced metal matrix composites. J Mater Process Technol 202:380-385.
12. Doraivelu SM, Gegel HL, Gunasekera JS, Malas JC, Morgan JT, Thomas Jr JF (1984) New yield function for compressible P/M materials. Int J Mech Sci 26:527-535.
13. Kuhn HA, Downey CL (1974) How flow and fracture affect design of preforms for powder forging. Int J Powder Metall Powder Technol 10:59-66.
14. Bao Y (2005) Dependence of ductile crack formation in tensile test on stress triaxiality, stress and strain ratios. Eng Fract Mech 72:505-522.
15. Bao Y, Wierzbicki T (2004) On fracture locus in the equivalent strain and stress triaxiality space. J Eng Mater Technol 46:81-98.

16. Butuc MC, Gracio JJ, Barata da Rocha A (2006) An experimental and theoretical analysis on the application of stress-based forming limit criterion. Int J Mech Sci 48:414-429.
17. Lee SR, Lee YK, Park CH, Yang DY (2002) A new method of preform design in hot forging by using electric field theory. Int J Mech Sci 44:773-792.
18. Sedighi M, Tokmechi S (2008) A new approach to preform design in forging process of complex parts. J Mater Process Technol 197:314-324.
19. Rajeshkannan A, Narayan S (2009) Strain hardening behaviour in sintered Fe-0.8%C-1.0%Si-0.8%Cu powder metallurgy preform during cold upsetting. J Eng Mfg 223:1567-1574.
20. Ramesh B, Senthivelan T (2010) Formability characteristics of aluminium based composite-a review. Int J Eng Technol 2:1-6.
21. Simchi A (2003) Effects of lubrication procedure on the consolidation, sintering and microstructural features of powder compacts. Mater Des 24:585-594.
22. Narayanasamy R, Anandakrishnan V, Pandey KS (2008) Effect of carbon content on workability of powder metallurgy steels. Mater Sci Eng A 494:337-342.
23. Han HN, Oh KH, Lee DN (1995) Analysis of forging limit for sintered porous metals. Scripta Metallurgica et Materialia 32:1937-1944.
24. Lewis RW, Khoei AR (2001) A plasticity model for metal powder forming processes. Int J Plasticity 17:1659-1692.

Notation

C Carbon

Fe Iron

ε_θ True hoop strain

ε_z True axial strain

R Relative density

R_o Initial relative density

σ_z Axial stress

σ_θ Hoop stress

σ_r Radial stress

σ_{eff} Effective stress